The Solidification of Undercooled Melts *via* Twinned Dendritic Growth

K.I. DRAGNEVSKI, R.F. COCHRANE, and A.M. MULLIS

The solidification of undercooled Cu-x wt pct Sn (x = 1, 2, 3, or 4) alloys has been studied by a melt-encasement (fluxing) technique. It was found that below undercoolings of $\Delta T \approx 90$ K, the preferred dendrite growth orientation in each of these alloys was along the <111> direction: moreover, the 2 and 3 wt pct Sn alloys also displayed evidence of twinned growth. Above $\Delta T \approx 90$ K, the preferred growth direction returned to the more usual <100> orientation.

I. INTRODUCTION

DURING solidification, the crystallographic growth direction is determined by the slowest-growing planes. In most metals with cubic crystal structures, this would normally be expected to give rise to growth along the <100> direction. However, a number of cubic systems have been shown to undergo a change in growth direction from <100> through <110> to <111> as the growth velocity is increased and, in particular, this has been observed *in situ* in the transparent NH_4Cl-H_2O system.[1] It has been suggested that this type of behavior is due to a competition between the surface-energy anisotropy, which favors <100> growth at low velocity, and the kinetic anisotropy, which favors <111> growth at high velocity.[2] Such phenomena have also been observed in viscous fingering in Hele–Shaw cells.[3,4]

Commercially, a change in the crystallographic growth direction of a metal during solidification processing can lead to serious problems. One example of this is the formation of "feather grains" in the direct-chill casting of commercial Al alloys, which, due to their high anisotropy and nonuniform aspect after etching,[5] can significantly impair both the mechanical properties and surface finish of formed products. Crystallographic investigations by Henry *et al*.[6,7] have shown that feather grains in Al alloys are brought about by a change in the principal growth direction from <100> to <110>. Moreover, these structures appear to be twinned, with a {111} twin plane, although in Al-Mg alloys, <110> dendrites have also been observed growing without twin assistance.[8] However, relatively few systematic studies have been made into the conditions that give rise to this type of morphology. Morris and Ryvola[9] found that a minimum solute concentration is required for feather-grain growth, although the reasons for this are not firmly established. A number of authors have also found that high imposed thermal gradients tend to favor feather-grain growth, while Eady and Hogan[10] found that the frequency of feather grains peaks at intermediate velocities.

Recent years have seen great advances in the measurement of crystal growth kinetics and phase selection in undercooled melts. However, such very fruitful studies have not proved possible on Al alloys, partly because aluminum oxide acts as a good heterogeneous nucleant, preventing the attainment of a large undercooling. However, Al alloys are not the only system in which feather grains have been reported. In particular, they are also observed in some Cu alloys,[11] although this is not generally regarded as a major commercial problem. However, a number of previous studies have shown that Cu and many of its dilute alloys can be easily undercooled,[12] thus raising the possibility that the mechanism behind kinetically induced changes in growth direction and/or dendrite twinning can be investigated without undercooling Al-based melts.

Here, a melt-encasement (fluxing) technique has been used to study the velocity-undercooling relationship in samples of Cu-x wt pct Sn (x = 1, 2, 3, or 4) up to undercoolings of ΔT = 320 K. The resultant as-solidified samples have been subject to microstructural investigation and X-ray texture analysis in order to determine the preferred growth direction. In this way, the crystallographic growth direction can be systematically investigated as a function of both solute concentration and growth velocity (undercooling).

II. EXPERIMENTAL METHOD

Alloys were prepared from elemental Cu and Sn with a purity of 99.9999 pct (metals basis). Cu-Sn alloys were formed by arc melting under an inert atmosphere to ensure complete mixing of the components. Samples, in the size range of 3 to 5 mm, were subsequently weighed to ensure no mass loss during arc melting.

Undercooling experiments were performed within a stainless steel vacuum chamber evacuated to a pressure of 5×10^{-6} mbar and backfilled to 500 mbar with N_2 gas. Samples were heated, in fused quartz crucibles, by induction heating of a graphite susceptor contained within an alumina shell. Viewing slots were cut in the susceptor and alumina to allow the sample to be viewed through a window in the chamber. A melt encasement, within a soda lime glass flux, was employed to reduce the number of potential heterogeneous nucleation sites, allowing the attainment of high undercoolings. Temperature determination was by means of a k-type thermocouple positioned beneath the crucible, which had been thinned at the base to reduce the thermal lag between the sample and thermocouple. Cooling curves were obtained with the aid of a chart recorder. A schematic diagram of the experimental apparatus is shown in Figure 1. By heating the sample to its melting temperature, cooling, and repeating this

K.I. DRAGNEVSKI, Doctoral Student, R.F. COCHRANE, Lecturer, and A.M. MULLIS, Senior Lecturer, are with the Institute of Materials Research, University of Leeds, Leeds LS2 9JT, United Kingdom. Contact e-mail: a.m.mullis@leeds.ac.uk

Manuscript submitted July 29, 2003.

procedure, it was found that melting temperatures were reproducible to within ±5 K. On heating, the sample and flux were taken to 300 K above the melting temperature to ensure complete melting of the glass, encasement of the sample, and the removal of gas bubbles from the flux. The samples were subsequently cooled to a predetermined temperature before nucleation was triggered by touching the sample surface with a thin alumina needle. As shown in Figure 1, the trigger needle is located at the top of the apparatus so that is can be pushed through the flux at the open top end of the silica crucible. By careful alignment of the apparatus, the trigger point can reproducibly be set at the top of the sample.

Immediately following nucleation, rapid growth of the solid phase (recalescence) will proceed by way of a growth front that radiates out from the trigger point, with the undercooled liquid ahead of the growth front acting as a sink for the latent heat released. Consequently, the fraction of solid (f_s) formed during the initial recalescence phase will be approximately

$$f_s = \frac{c_p \Delta T}{H}$$

where c_p is the specific-heat capacity of the liquid and H is the latent heat of fusion for the alloy. The remaining liquid will solidify more slowly as the sample cools following recalescence. As, during recalescence, the solid grows close to the equilibrium melting temperature, the portion of the sample behind the growth front will be hotter (and, hence, brighter) than the remaining undercooled liquid. At the high growth velocities encountered with metallic melts undercooled by more than 50 K, the thermal boundary layer is very thin (typically <1 μm), giving the appearance of bright front with a sharp interface moving radially out from the trigger point. As the position of the trigger point is known, the linear velocity of the growth front can be determined by measuring the rate at which this bright front propagates across the surface of the sample.

The measurement of growth velocities is performed using a 16-element linear photo-diode array, allowing the time taken for the bright recalescence front to move across the relatively dark sample to be measured. Light from the sample is passed through a beam splitter that distributes the light between a charge-coupled device (CCD) camera and the photodiode array. The CCD camera allows accurate sample positioning and focusing. It is also possible *via* this arrangement to measure directly the dimension of the sample along the photodiode axis. A current proportional to the light intensity falling on each photodiode is produced, which is then amplified and recorded. Each of the 16 photodiodes has an independent, fast-settling, low-noise, Dielectrically Isolated Field Effect Transistor (DIFET) amplifier with a current to voltage gain of 10^6 V A^{-1}. The signals are then passed, *via* switching circuitry, to a pair of voltage adders for output. The output signal is displayed as a light-intensity against time trace on a digital-storage oscilloscope, from which the rate at which the solidification front moves across the sample can be determined. The raw data than undergo a geometrical correction to allow for the fact that the velocity of the three-dimensional growth front is actually measured on a two-dimensional imaging plane.[13] The accuracy of this technique and the radial growth of the solidification front were verified using high-speed digital imaging (up to 40,500 fps) to track the progress of the recalescence front directly.[14]

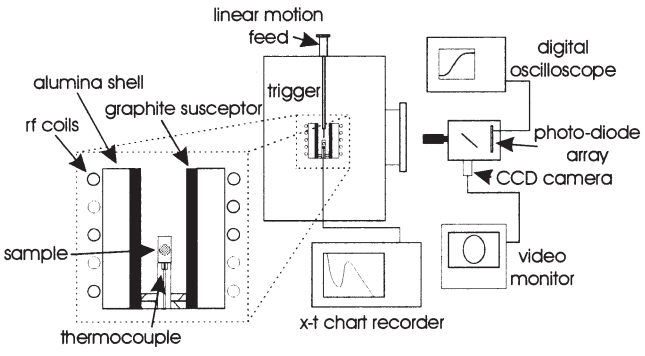

Fig. 1—Schematic diagram of the melt fluxing apparatus used.

The as-solidified samples were subsequently sectioned for analysis using optical microscopy and X-ray texture analysis. As the trigger point on the sample is known and the growth front propagates radially out from this point, sections can be cut with a well-defined orientation relative to the growth direction. Figure 2 illustrates optical micrographs of both longitudinal and transverse sections through a sample. In the longitudinal section, well-defined dendrites are apparent running the length of the specimen. These have a strong horizontal/vertical orientation, illustrating that the dendrite growth direction is aligned with the inoculation needle. Transverse sections taken from the center of the sample will, thus, generally be orthogonal to the principal growth direction. An X-ray texture analysis on such sections has been used to determine the crystallographic orientation of the primary dendrites (which will be apparent as a pole located at the center of an appropriate texture map).

Optical microscopy was performed on polished sections using a NIKON* Optiphot microscope in differential-interference contrast (DIC) and bright-field modes, the samples having been etched in ammonium persulphate (100 g/L) to reveal the dendritic substructure. The X-ray pole-figure plots were generated using a PHILIPS** APD1700 diffractometer (Cu K_α radiation) equipped with a texture stage.

*NIKON is a trademark of Nikon Corp., Kanagawa, Japan.

**PHILIPS is a trademark of Philips Electronic Instruments Corp., Mahwah, NJ.

III. RESULTS

Velocity-undercooling curves for the four alloys studied, plotted on log-log axes, are shown in Figures 3(a) through (d). In each case, two distinct power-law trends of the form $V \propto (\Delta T)^\beta$ are apparent. At low undercoolings, typically less than ≈85 K, the growth velocity increases quite slowly with undercooling, the exponent β increasing systematically with Sn concentration from 0.50 for Cu 1-wt pct Sn to 1.53 for Cu-4 wt pct Sn. Above $\Delta T \approx 85$ K, a much more rapid increase in growth velocity occurs. For $x = 1$, 2, or 3 wt pct, the value of β shows remarkable consistency, being 3.54 ± 0.02, while for $x = 4$ wt pct, a smaller exponent of $\beta = 2.32$ is found. We will denote here the undercooling at which the two curves intersect as $\Delta T'$.

Velocity-undercooling curves of this type have previously been reported for other systems. In Ni-Cu, Eckler and Herlach[15]

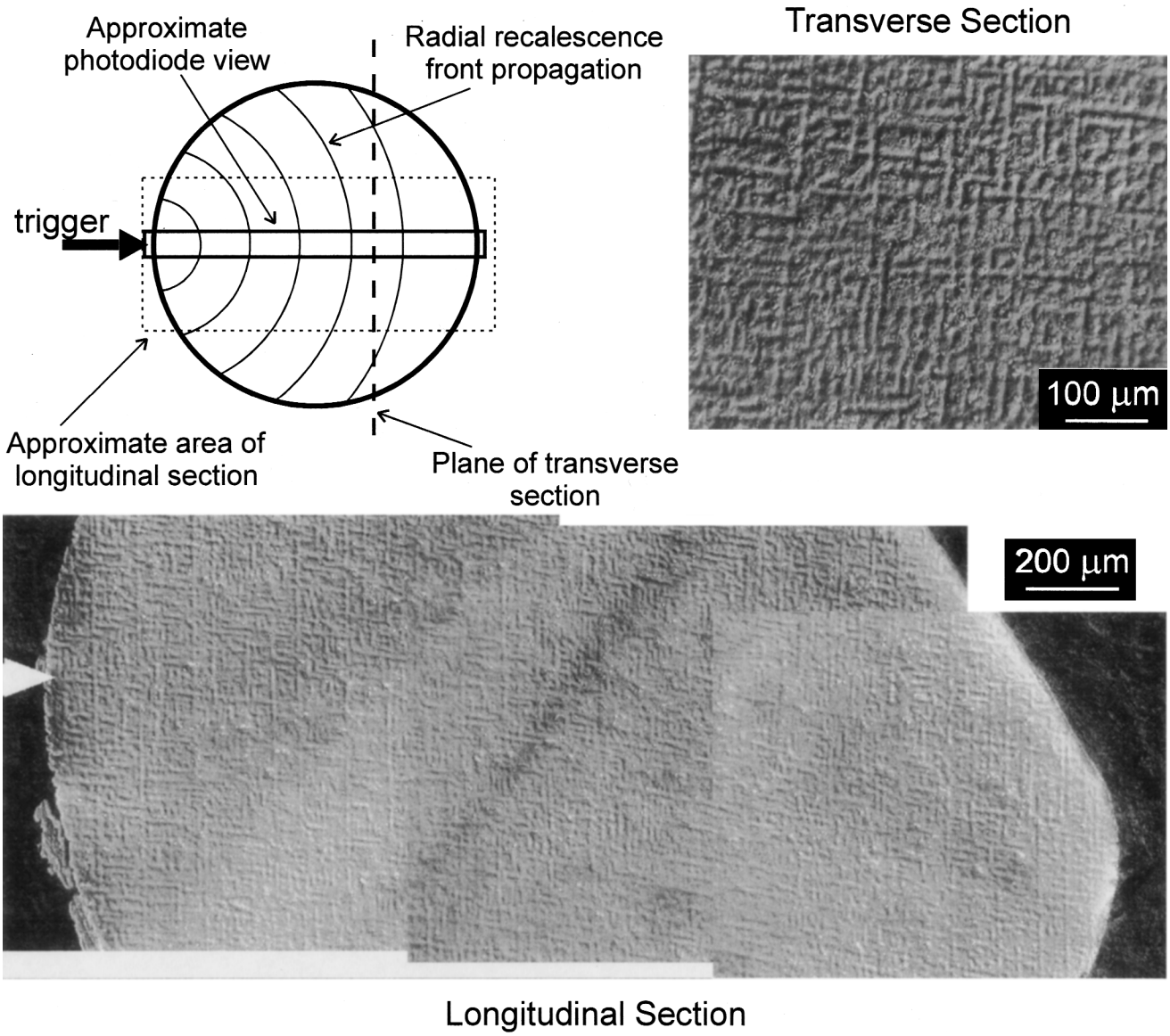

Fig. 2—Schematic representation of the progress of the recalescence front in an undercooled droplet, with examples of microstructures obtained from both longitudinal and transverse polished sections. The notch on the longitudinal section indicates the position at which the inoculation needle touched the surface. Also shown is the approximate field of view of the photo-diode array used to make velocity determinations.

have proposed that the effect may be produced by fluid-flow effects in the melt. However, Ni-Cu undergoes spontaneous grain refinement at low undercoolings, whereby the original structure formed during the recalescence phase is subject to remelting.[16,17,18] Although grain refinement is likely to be an unrelated effect, remelting renders microstructural investigation of the as-solidified samples of little value. In contrast, Cu-Sn does not exhibit grain refinement at low undercoolings, allowing detailed evaluation of the as-solidified microstructure, which here has been performed by optical microscopy on polished and etched sections and by X-ray texture analysis.

The most straightforward region to explain is that above $\Delta T'$, as the results of the microstructural and texture analysis are essentially independent of composition. Figure 4 shows an optical micrograph of one such sample, in this case taken from a transverse section of a Cu-3 wt pct Sn alloy solidified at an undercooling of $\Delta T = 91$ K, marginally above $\Delta T'$. Strong orthogonality at the junctions of the dendrite arms is apparent, giving rise to the classic <100> dendritic microstructure. That we are observing simple <100> growth can be confirmed by X-ray texture analysis. Figures 5(a) and (b) show the {111} and {100} texture maps for the sample, respectively. The {111} map shows four poles, each of which is located close to 54 deg, with each pole being rotated from its neighbor by 90 deg. The {100} map shows three poles, one which (pole 1) lies at the center of the plot. For a transverse section orthogonal to the principle growth direction, this is indicative that the crystallographic orientation of the dendrite is <100>. The remaining two poles are at a radial distance of 90 deg from the central pole and are rotated from each other by 90 deg. Again, this is exactly as would be expected for the growth of a single-crystal dendrite along the <100> direction. Generally similar results were obtained for all alloy compositions at undercoolings above $\Delta T'$, up to the highest undercooling achieved ($\Delta T = 320$ K). This is illustrated in

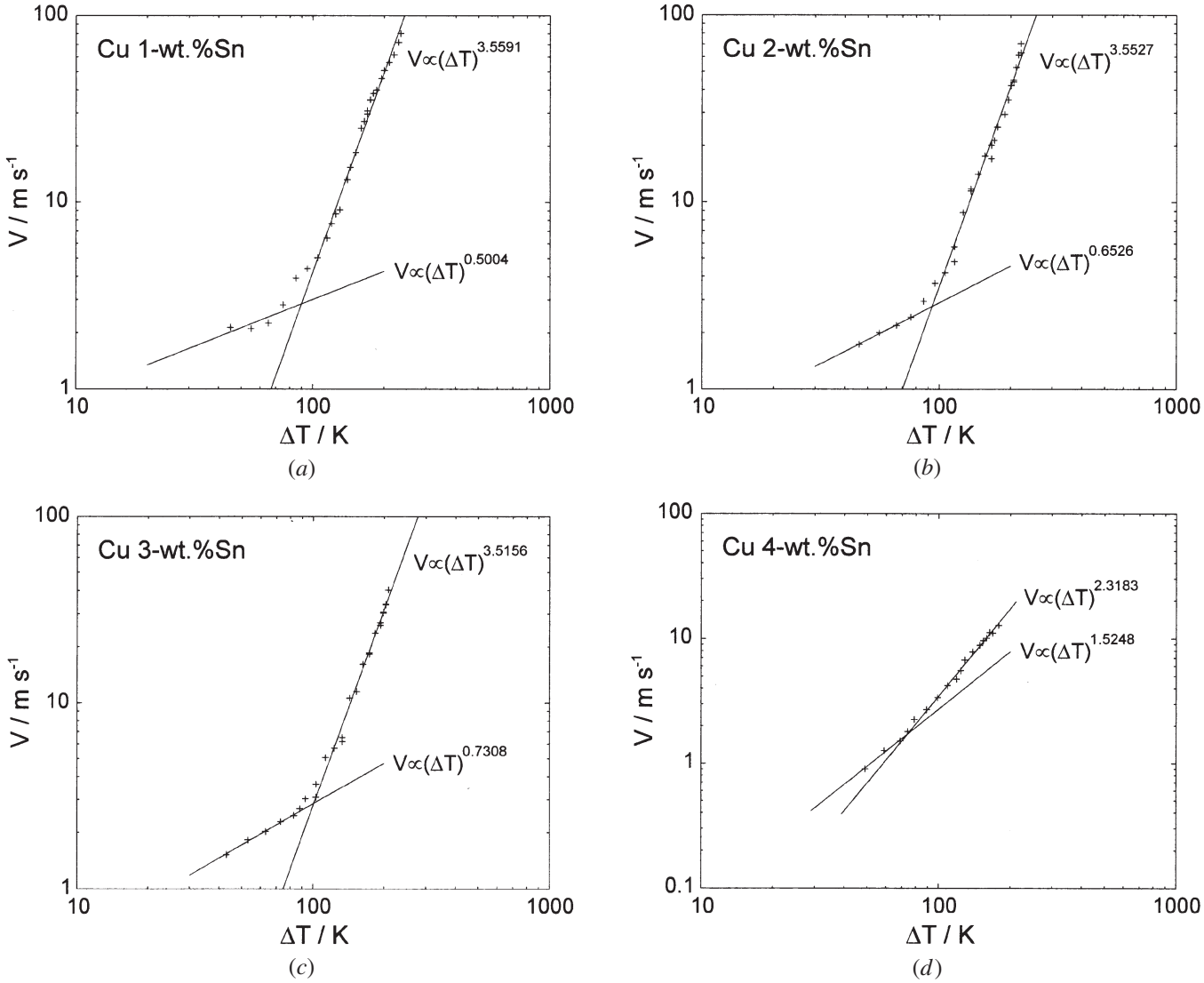

Fig. 3—(*a*) through (*d*) Velocity-undercooling curves for Cu-1, 2, 3, and 4 wt pct Sn alloy, showing two distinct growth regimes.

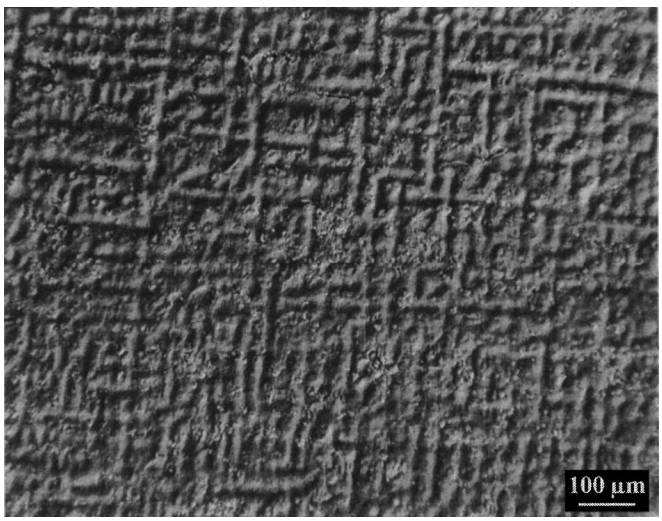

Fig. 4—Optical micrograph of Cu-3 wt pct Sn alloy undercooled by ΔT = 91 K prior to nucleation, displaying strong orthogonality at the junctions of the dendrite arms.

Figures 6(a) and (b), which show the microstructure of a Cu-3 wt pct Sn alloy at an undercooling of $\Delta T = 266$ K. Under DIC-mode optical microscopy (Figure 6(a)), the orthogonal dendritic structure is still apparent, although much finer than at lower undercoolings, as would be expected from dendrite growth theory. The sample is not, however, grain refined. As can be seen from the bright-field image of the same sample (Figure 6(b)), only two grains occupy the whole field of view.

Below $\Delta T'$, the situation is less straightforward, as there are significant variations in the behavior of the system with composition. Figure 7 shows the microstructure of a transverse section taken from a sample of the Cu-1 wt pct Sn alloy undercooled by 75 K prior nucleation. The low solute content leads to very low contrast between the dendrites and the interdendritic regions in the sample, but even so, some substructure is evident. It is, however, quite different in nature from the large orthogonal arrays of dendrites seen above $\Delta T'$, instead comprising many dots, giving the sample what we might term an orange-peel appearance. The texture analysis from this sample is, however, revealing. Figure 8 shows the {111} pole-figure plot for this sample. This shows the four {111}

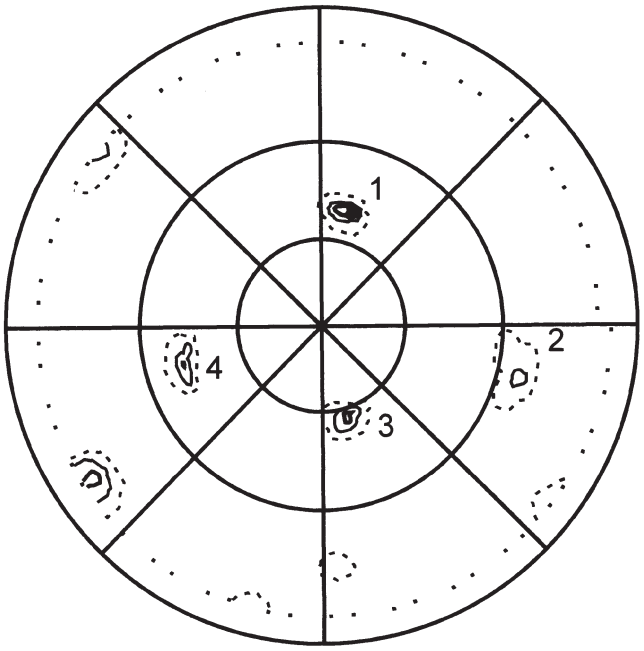

(*a*)

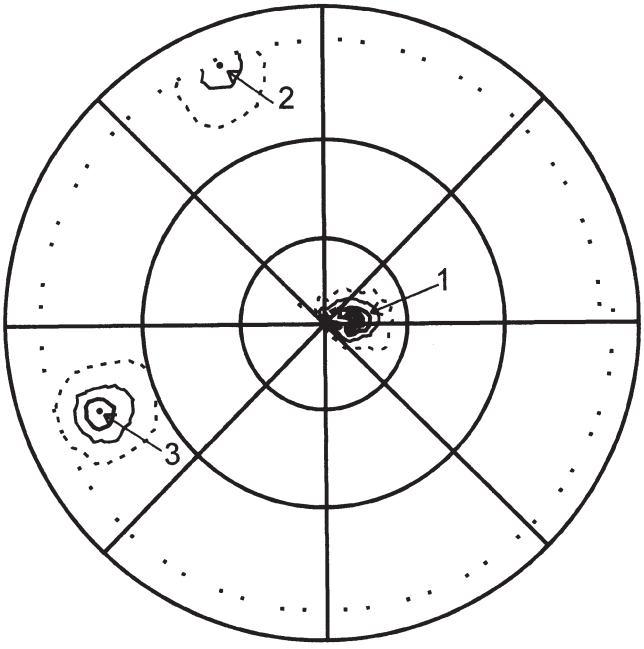

(*b*)

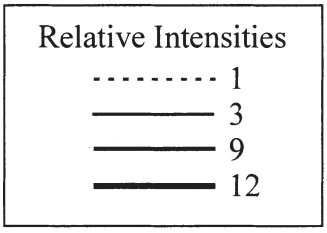

Fig. 5—(*a*) <111> and (*b*) <100> texture maps for Cu-3 wt pct Sn alloy undercooled by $\Delta T = 91$ K prior to nucleation, indicating growth along the <100> direction.

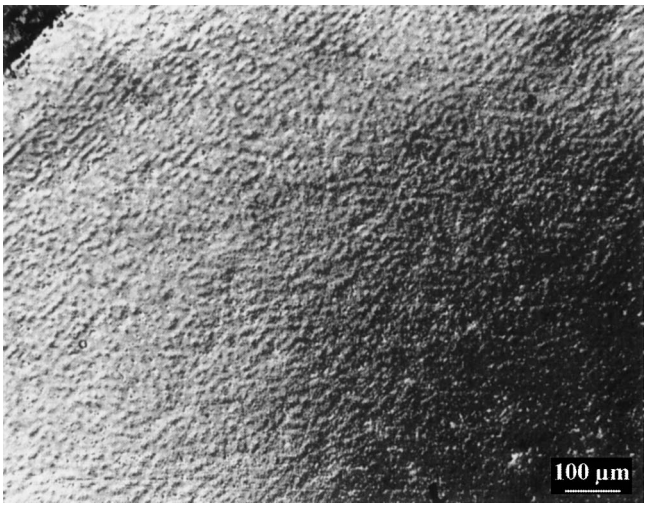

(*a*)

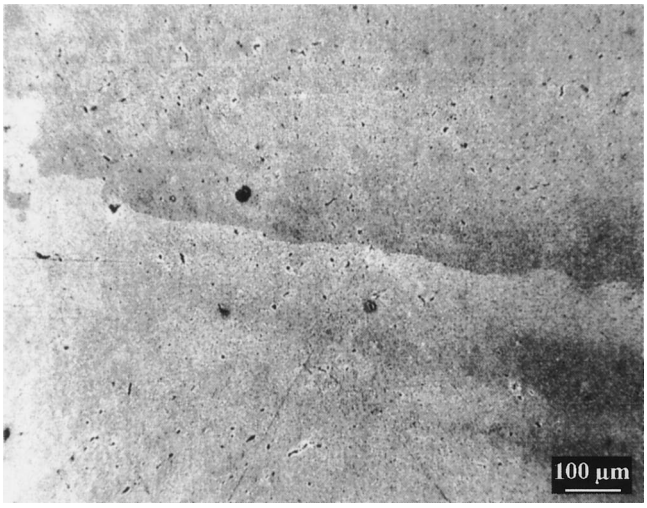

(*b*)

Fig. 6—Optical micrograph of Cu-3 wt pct Sn alloy undercooled by $\Delta T = 266$ K prior to nucleation in (*a*) DIC mode revealing a fine but regular dendritic substructure and (*b*) bright field showing a coarse grain structure.

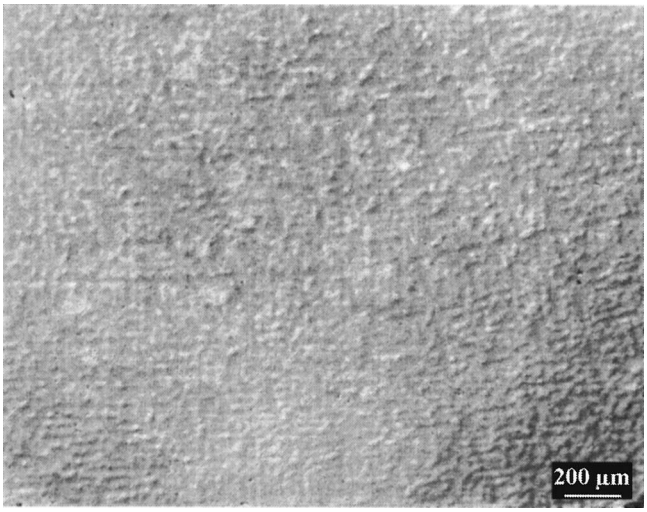

Fig. 7—Micrograph taken from a transverse section of a Cu-1 wt pct Sn alloy undercooled by $\Delta T = 75$ K prior to nucleation.

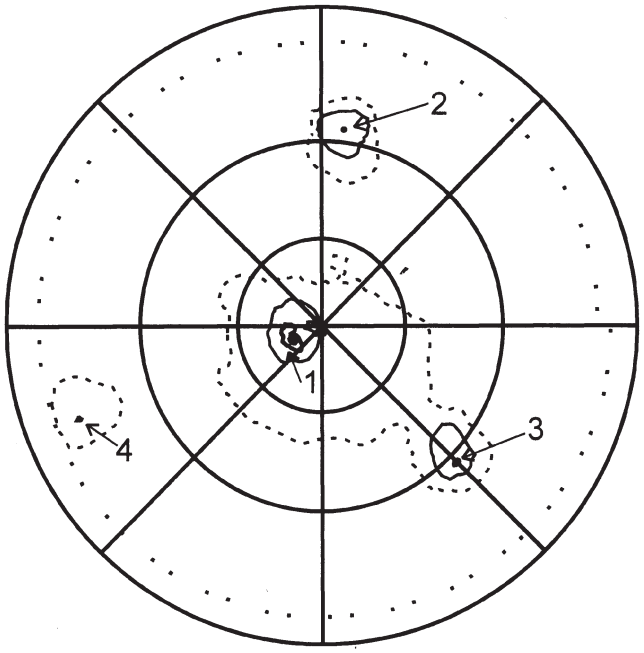

Fig. 8—<111> texture map for Cu-1 wt pct Sn alloy undercooled by ΔT = 75 K prior to nucleation clearly demonstrating growth along the <111> direction. Intensity contours are the same as in Fig. 5.

poles, one of which is at the center, clearly indicating the <111> growth direction, while the other three at 72 deg, 53 min have the expected threefold symmetry. As a result of the primary growth direction being <111>, we should not be surprised that our transverse section does not show particularly clear evidence for a dendritic array. For <100> growth, the secondary dendrite arms are orthogonal to the primary. Consequently, when a transverse section is cut, an array of secondary arms should lie in the plane of the section. However, for <111> growth, the angle between the primary and secondary arms will be 72 deg, 53 min, so that when the transverse section is cut, the secondary arms will intersect the plane of the section at an angle. This is likely to give rise to a series of dots or short sections of dendrite, not unlike the view seen in Figure 7. Based on the microstructural and texture-analysis evidence, we would thus conclude that for a Cu-1 wt pct Sn alloy below $\Delta T'$, solidification proceeds by the growth of dendrites along the <111> direction, while above $\Delta T'$, the primary growth direction is <100>. It would also seem likely that the different velocity-undercooling relationships observed above and below $\Delta T'$ reflect the different crystallographic orientations of the dendrites in these growth regimes.

In Cu-2 wt pct Sn, a somewhat different pattern emerges. An example microstructure taken from a sample undercooled by $\Delta T = 82$ K is shown in Figure 9. As with the Cu-1 wt pct Sn alloy, the microstructure observed in the transverse section lacks contrast between the dendritic and interdendritic regions after etching due to the low solute concentration, and this makes interpretation difficult. However, despite the low contrast, a number of features can be identified as sections of a dendritic array. Of particular interest are the features marked with arrows, which seem to be intersections between dendritic arms with angles in the range of 25 to 35 deg. As before, X-ray texture analysis pro-

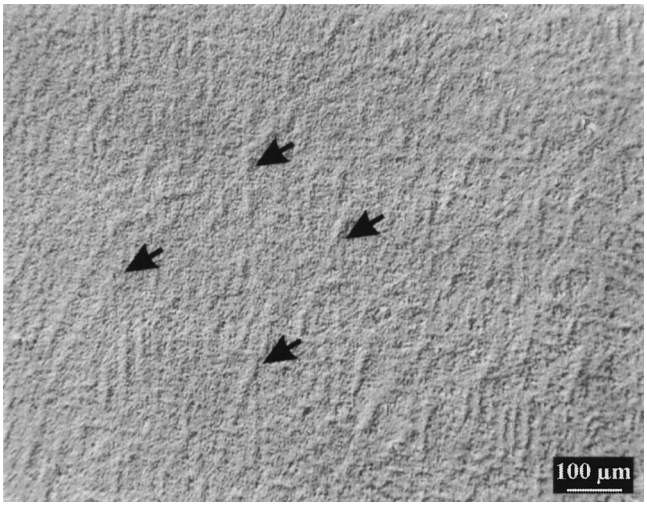

Fig. 9—Micrograph taken from a transverse section of a Cu-2 wt pct Sn alloy undercooled by ΔT = 82 K prior to nucleation. Arrows indicate regions where dendritic features appear to have intersections with angles in the range 25 to 35 deg.

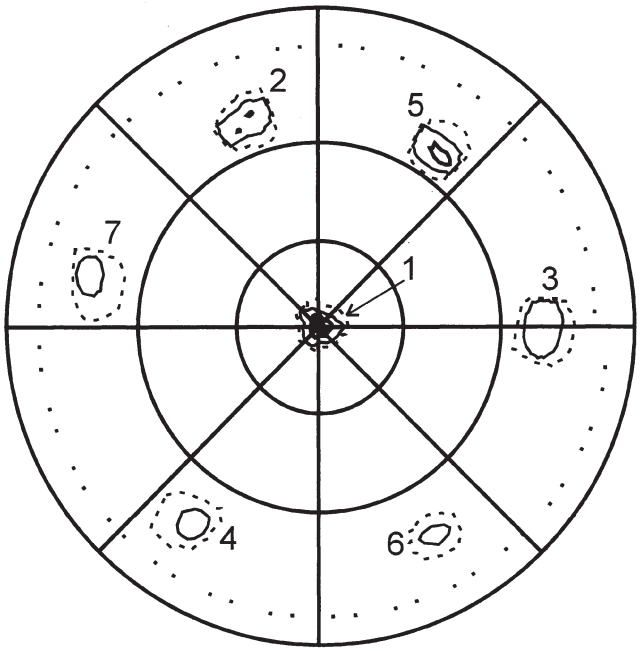

Fig. 10—<111> texture map for Cu-2 wt pct Sn alloy undercooled by ΔT = 82 K prior to nucleation. Intensity contours are the same as in Fig. 5.

vides definite clues as to the growth mode in the sample, albeit that this is different from that observed in the Cu-1 wt pct Sn alloy. The {111} texture map for this sample is shown in Figure 10. As with the Cu-1 wt pct Sn alloy, there is a strong pole (pole 1) at the center of the texture map, indicating that the primary growth direction is again <111>. There are, however, now seven poles in total, not four. All of the poles lie close to 72 deg, 53 min and display a sixfold rotation symmetry. Consequently, if we divide these poles into two groups of four by using pole 1 twice (*i.e.*, poles 1, 2, 3, 4 and 1, 5, 6, 7), we can see that the poles lie approximately at the vertices of two equilateral triangles,

rotated from each other by 60 deg. This pattern suggests that we have the growth of two orientationally related {111} crystals, as might occur if we have either a twinned dendrite or a stacking-fault sequence in the primary dendrite. Consequently, it appears that we can again conclude that above $\Delta T'$, solidification proceeds by the growth of dendrites along the <100> direction, while below $\Delta T'$, the growth direction is <111>. However, in the case of Cu-2 wt pct Sn, there appears to be a tendency toward twin-assisted growth or the formation of stacking-fault sequences.

Figure 11 shows a micrograph of a transverse section through a sample of the Cu-3 wt pct Sn alloy, undercooled by ΔT = 48 K prior to nucleation. In contrast to the sections taken from the 1 and 2 wt pct Sn alloys, etching the more-concentrated alloy now clearly reveals the substructure with high contrast between the dendrites and the interdendritic regions. As described previously, the transverse section will lie approximately orthogonal to the growth direction, a fact which is confirmed subsequently by X-ray texture analysis. However, the coarse dendritic substructure, which is now clearly visible, appears to be highly irregular. In particular, there are a number of features which can be identified as being the intersection of two dendrite arms, in which the angle of intersection is ≈60 deg. To further elucidate the dendrite growth mechanism in the sample, a {111} texture map has been generated, which is shown in Figure 12. We note from this that there are four strong {111} poles (numbered 1 through 4 on the figure). One of these is close to the center of the pole figure (pole 1), while the other three are close to 72 deg, 53 min and display threefold rotational symmetry. As before, both of these facts would suggest that the primary growth direction was <111>, not <100>. The small departure of pole 1 from the center of the pole figure probably indicates that the inoculation needle was slightly off-axis and, so, did not touch the sample exactly on its top surface. However, in addition to the four strong poles already discussed, there are also three weaker poles. The occurrence of seven poles is suggestive that we are again observing twinning or a stacking-fault sequence, as was the case for the Cu-2 wt pct Sn alloy. However, poles 5 through 7 are not only weaker than poles 2 through 4, but occur at a smaller angle. As poles 5 through 7 in this figure are rather diffuse, we have investigated further samples of this alloy in order to ascertain the origin of these poles.

The microstructure obtained from a transverse section of a Cu-3 wt pct Sn alloy sample undercooled by ΔT = 83 K is shown in Figure 13. The dendritic substructure is still highly irregular and, indeed, over large areas of the section, a clear dendritic array is not clearly visible. The {111} texture map (Figure 14(a)) again displays seven poles, although these are rather better developed than at ΔT = 48 K, allowing accurate determination of their positions. Again, one of the poles is located close to the center of the figure, indicating a <111> growth direction, while poles 2 through 4 are close to 72 deg, 53 min and display threefold rotational symmetry. Poles 5 through 7 do not follow this trend. However, by using a Wulff net to measure the angle between pole 4 and the center of the pole-figure

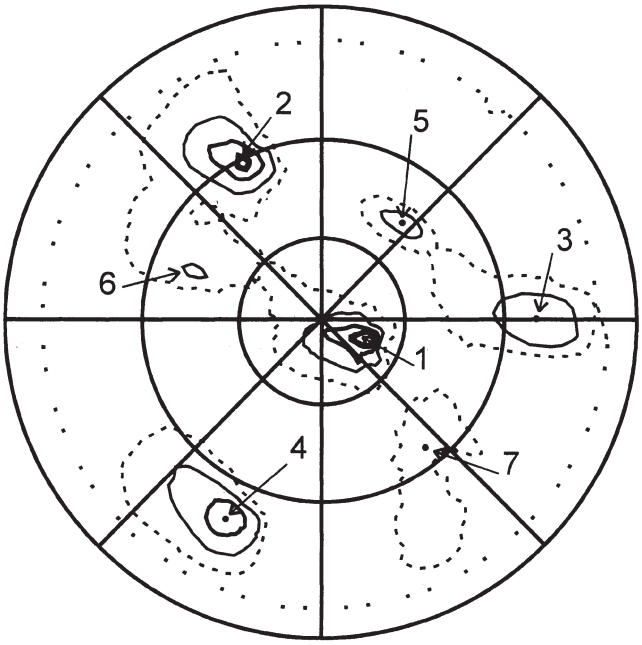

Fig. 12—<111> texture map for Cu-3 wt pct Sn alloy undercooled by ΔT = 48 K prior to nucleation. Intensity contours are the same as in Fig. 5.

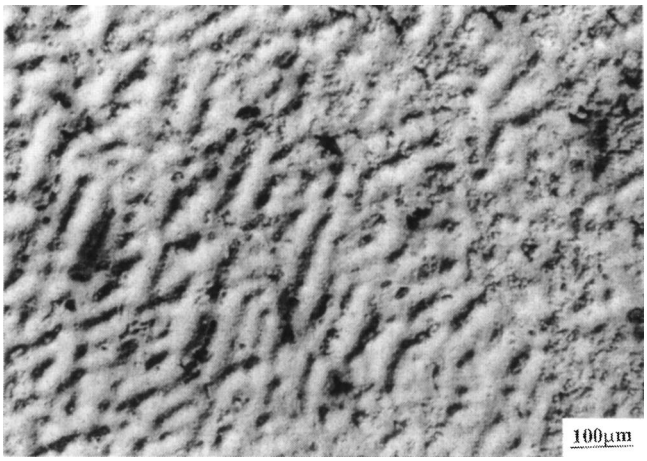

Fig. 11—Micrograph taken from a transverse section of a Cu-3 wt pct Sn alloy undercooled by ΔT = 48 K prior to nucleation.

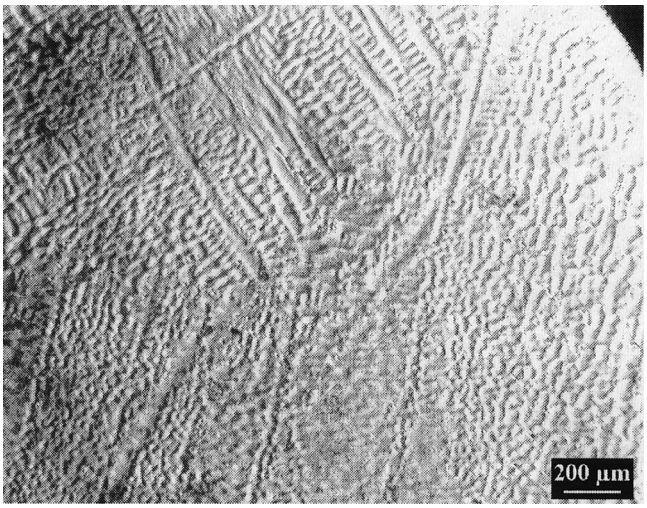

Fig. 13—Micrograph taken from a transverse section of a Cu-3 wt pct Sn alloy undercooled by ΔT = 83 K prior to nucleation.

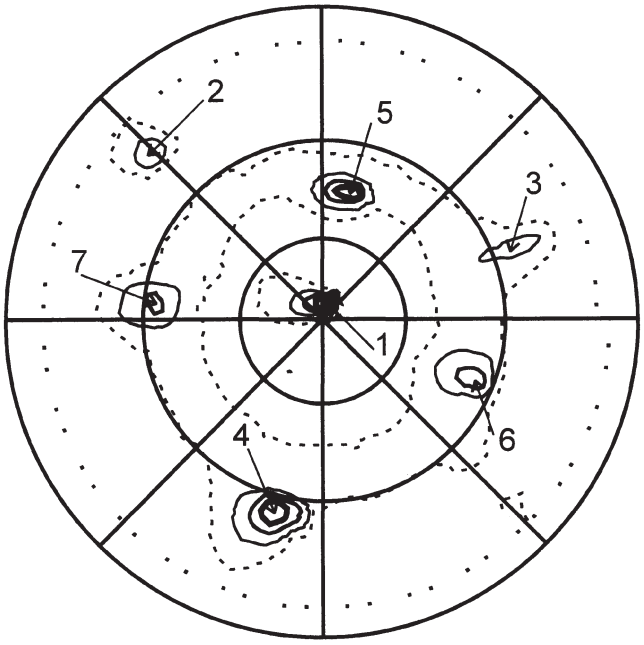

(*a*)

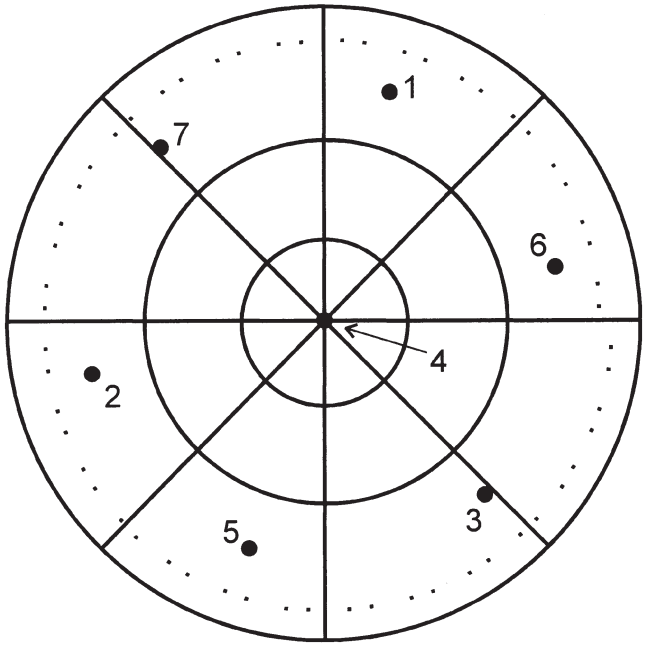

(*b*)

Fig. 14—(*a*) <111> texture map for Cu-3 wt pct Sn alloy undercooled by $\Delta T = 83$ K prior to nucleation. Intensity contours are the same as in Fig. 5. (*b*) Schematic illustration of the effect of using a Wulff net to measure the angle between pole 4 and the center of the pole figure plot shown in (a), so that each pole can be rotated by the same angle along small circles.

plot, each pole can be rotated by the same angle along small circles, allowing Figure 14(a) to be redrawn as in Figure 14(b), with pole 4 at the center. It is now apparent that there are two orientationally related crystals, but that pole 4 is the common pole, not pole 1, with a common angle between the poles of either 72 deg, 53 min or 109 deg, 47 min (*i.e.*, there are two sets of four poles; 1, 2, 3, 4 and 4, 5, 6, 7). This would indicate that twinning, or the formation of a stacking-fault sequence, has occurred not about the primary growth direction, but about one of the secondary directions. The most likely scenario is that a single {111} crystal was initially nucleated by the inoculation needle, growing approximately orthogonal to the section taken. However, during the growth process, twinning or the formation of a stacking-fault sequence has occurred on one of the secondary arms, giving rise to a second, orientationally related crystal.

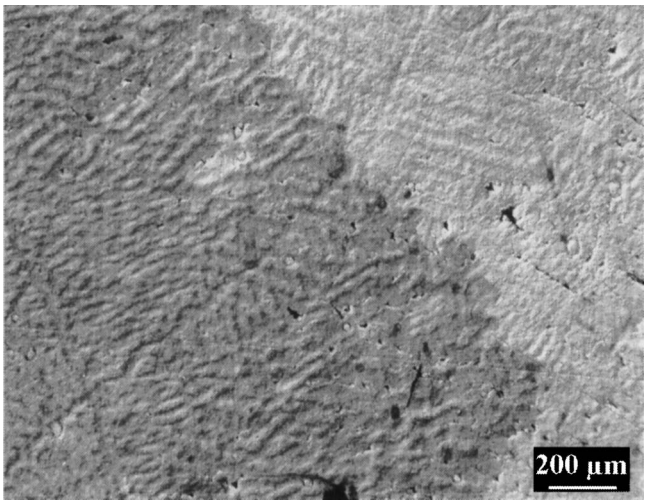

Fig. 15—Micrograph taken from a transverse section of a Cu-4 wt pct Sn alloy undercooled by $\Delta T = 65$ K prior to nucleation.

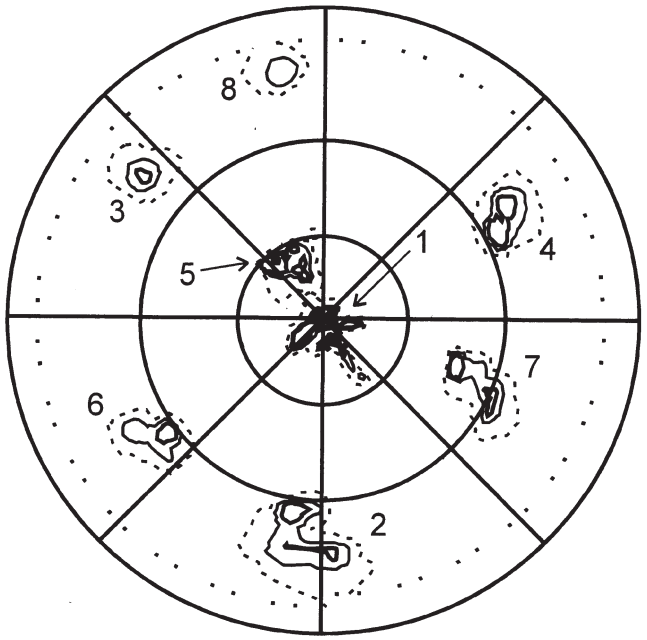

Fig. 16—<111> texture map for Cu-4 wt pct Sn alloy undercooled by $\Delta T = 65$ K prior to nucleation. Intensity contours are the same as in Fig. 5.

Finally, we turn to the Cu-4 wt pct Sn alloy. The microstructure obtained from a transverse section of a sample of this alloy, undercooled by $\Delta T = 65$ K, is shown in Figure 15. In many respects the microstructure appears very similar to that for the Cu-4 wt pct Sn alloy, with a coarse and highly irregular dendritic substructure. In this sample, however, there are very clearly two grains present. This is also clearly seen in the <111> pole figure, reproduced as Figure 16. There are now

eight poles, which we can group into two sets of four. Pole 1 is located at the center of the figure and poles 2 through 4 have a common angle with this pole which is close to 72 deg, 53 min. Pole 5 is also close to the center of the texture map, and, if the figure is reploted on a Wulff net so as to rotate pole 5 into the center, poles 6 through 8 again have a common angle close to 72 deg, 53 min with this pole. There is however, no specific orientational relationship between the two sets of poles 1 through 4 and 5 through 8. We would, therefore, conclude that in this instance there have been two independent nucleation events giving rise to two unrelated grains. This may have occurred if the inoculation needle broke as it were pushed through the flux layer and, consequently, touched the sample surface in two places near the top of the sample.

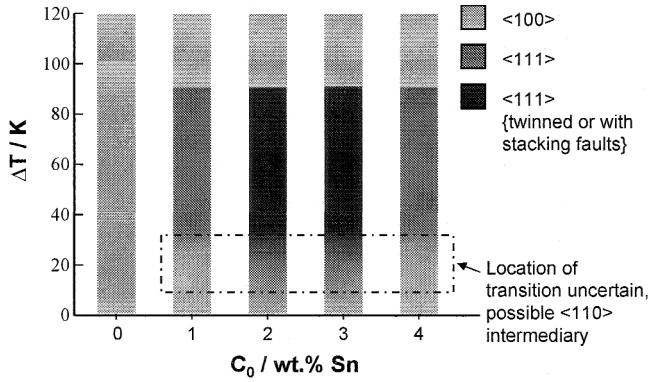

Fig. 17—Summary of the preferred growth directions for pure Cu and Cu-1, 2, 3, and 4 wt pct Sn alloy as a function of undercooling.

IV. DISCUSSION

The experimental evidence presented earlier indicates that during the solidification of a Cu-x wt pct Sn ($x = 1$, 2, 3, or 4) alloy from its undercooled melt, the preferred growth direction below $\Delta T'$ is <111>, while above $\Delta T'$, the preferred growth direction is <100>. Moreover, for $x = 2$ and 3 wt pct, growth along the <111> direction is accompanied by a higher tendency toward either twinning or the formation of stacking-fault sequences. We have not studied the solidification of these systems at very low undercoolings ($\Delta T < 40$ K) directly using the fluxing method, due to difficulty in nucleating solidification of fluxed samples at low undercoolings. Moreover, it also becomes very difficult at low undercoolings to make growth-velocity measurements, there being little contrast at the recalescence front due to the small volume fraction transforming from the liquid to the solid phase. However, normal casting experiments indicate that as equilibrium is approached ($\Delta T < 10$ K), solidification proceeds by the growth of dendrites along the <100> direction. Consequently, the growth of dendrites along the <111> direction is likely to be restricted to a narrow window of undercoolings, which is unlikely to exceed 10 to 90 K. Moreover, evidence from other systems suggests that there may also be an intermediate transition between <100> growth and <111> growth, in which the dendrite trunks are directed along the <110> direction, although we have not observed this directly in Cu-Sn. In a similar study of pure Cu, we found that the <100> growth direction was maintained at all undercoolings,[12] and we might, thus, deduce that a minimum solute concentration is required in order to initiate the switch to <111> growth. The observed phase transitions are summarized in Figure 17. For all four alloy compositions studied here, the change in the growth direction has a clear signature in the velocity-undercooling curve when this is plotted on log-log axes. For all compositions, the fastest-growing mode dominates.

Interestingly, a number of strongly faceting systems show behavior analogous to that observed here in Cu-Sn alloys. Battersby *et al.*[19] have showed that in dilute Ge-Fe alloys, undercooled by the fluxing technique, growth along the <111> direction at low undercoolings ($\Delta T < 150$ K) is replaced by growth along the <100> direction at higher undercoolings. This switch in the growth direction was coincident with a transition from faceted to continuous growth with increasing undercooling. Moreover, many of the <111> texture maps for this system were remarkably similar to those shown for the Cu-2 wt pct Sn and Cu-3 wt pct Sn systems, in that they displayed seven poles, with a pole at the center of the figure and a common angle between the poles close to 72 deg, 53 min or 109 deg, 47 min.

Unlike Cu-Sn, though, the strongly faceted nature of the Ge-Fe system at low undercoolings made it possible for Battersby to identify a large number of growth twins in the polished sections.[13] This has not been the case here, where we have not been able to identify any twin planes in our sections, whether transverse or longitudinal. However, given that none of the Cu-Sn systems have shown any faceted character, this is maybe not surprising.

Kuribayashi and Aoyama[20] have also observed <111> growth in electromagnetically levitated Si below undercoolings of 100 K, although they do not report if there was a change in the growth direction at higher undercoolings, where continuous growth was observed. It is not clear whether the transition will be observed in pure semiconductors or, as with metals, whether some solute is required. Kuribayashi and Aoyama claim to have used pure Si, although the presence of visible dendrites within their samples would strongly suggest that some solute was present.

Even given that we have not been able to identify specific twin planes in our sections, there are still reasons to believe that we are observing dendritic twinning and not simply a stacking-fault sequence. First, the close similarity of the X-ray texture maps for Ge-Fe and Cu-Sn (compare, for instance, our Figure 14(a) with Figure 5 in Reference 19) provides at least indirect support for this view. Second, the formation of two orientationally related crystals was seen in all our samples undercooled below $\Delta T'$ in the Cu-2 wt pct Sn and Cu-3 wt pct Sn alloys and not at all in the Cu-1 wt pct Sn and Cu-4 wt pct Sn alloys. As the creation of a stacking-fault sequence is an essentially random occurrence, the consistent observation of orientationally related crystals at a particular concentration is, thus, likely to be indicative of twinning. If twinning conveys a growth advantage at a particular concentration, the twinned crystal should always dominate the growth process. Conversely, a stacking-fault sequence would be expected to be present in some samples but absent in others. Finally, the previous observation of feather grains in Cu alloys[11] indicates that twinning in this material might well be expected.

The analogous behavior of the semiconductors Ge and Si with the Cu-Sn systems studied here might be taken as

evidence that growth in Cu-Sn does not take place at a truly continuous interface, but rather that there are some characteristics of faceted growth present. This is despite the fact that none of the microstructures presented here for Cu-Sn alloys display any features which would normally be associated with faceted growth. However, it would be consistent with the observation of twinned growth in the 2 and 3 wt pct Sn alloys, the concept of twin-assisted growth being somewhat at odds with the conventional view of a continuous dendrite.

Indeed, despite the importance of dendritic twins in industrial casting practice, there is no general consensus as to the morphology of a twinned dendrite. Wood *et al.*[21] have argued that a stable morphology would be for the dendrite to display a sharper-than-normal tip with the twin plane emanating from the point. Conversely, Henry *et al.*[7] have suggested that a twin dendrite would display a split or grooved tip, with the twin plane running down the trunk from the grove. This type of morphology might be brought about when the principal directions of the surface-energy and kinetic anisotropies do not coincide. A competition between the surface-energy anisotropy favoring <100> growth at low velocity and the kinetic anisotropy favoring <111> growth at high velocity would also explain why <111> growth is observed at intermediate undercoolings, but not as equilibrium is approached. However, in the case of Cu-Sn, this cannot offer a full explanation of the observations, as the switch back to the <100> direction as the growth velocity is increased further is not explained.

In light of the results presented here, we would suggest that future models of twinned dendritic growth consider the possibility of growth structures that are intermediate between the classical faceted crystal and the fully continuous dendrite.

V. SUMMARY

In summary, the results presented here for Cu-Sn alloys are consistent with the known facts for feather-grain formation, even if the exact mechanism giving rise to this type of morphology is not fully understood. A minimum solute concentration is required to induce either a change in the growth direction or dendrite twinning. In high-purity Cu, we found no evidence of growth along the <111> direction at any undercooling. The minimum concentration of Sn required to initiate a change in direction is unknown, but is clearly less than 1 wt pct. However, exactly what role the solute plays in either bringing about a change in the growth direction or initiating twinning is unknown.

Both the change in growth direction and twinning seem to be restricted to an intermediate range of undercoolings and, hence, growth velocities. In Cu-Sn alloys, <100> growth in the near-equilibrium range of undercoolings is replaced by <111> growth somewhere below $\Delta T < 40$ K, although we have not been able to probe this region directly. Whether there is a <110> transition before the switch to <111> growth is also unknown. However, it is clearly established from the results presented here that the upper limit to <111> growth is around $\Delta T = 90$ K, with a switch back to the <100> growth direction being observed at all undercoolings above this level. For the alloy compositions reported here, this corresponds to growth velocities in the range 3 to 3.5 m s^{-1}, which is in the region where solute trapping might be expected to become dominant. Given that pure systems do not appear to display either a change in growth direction or twinning, it is tempting to suggest that the transition back to the <100> growth direction in the Cu-Sn alloy above $\Delta T = 90$ K is due to a switch to partitionless growth.

REFERENCES

1. K.A. Gudgel and K.A. Jackson: *J. Cryst. Growth*, 2001, vol. 225, pp. 264-67.
2. S.K. Chan, H.H. Reimer, and M. Kahlweit: *J. Cryst. Growth*, 1976, vol. 32, pp. 303-10.
3. E. Ben-Jacob, R. Godbey, N.D. Goldenfeld, J. Koplik, H. Levine, T. Mueller, and L.M. Sander: *Phys. Rev. Lett*., 1985, vol. 55, pp. 1315-18.
4. E. Ben-Jacob and P. Garik: *Nature*, 1990, vol. 343, pp. 523-30.
5. D.A. Granger and J. Liu: *JOM*, 1983, June, pp. 54-59.
6. S. Henry, T. Minghetti, and M. Rappaz: *Acta Mater*., 1998, vol. 46, pp. 6431-43.
7. S. Henry, P. Jarry, and M. Rappaz: *Metall. Mater. Trans. A*, 1998, vol. 29A, pp. 2807-17.
8. S. Henry and M. Rappaz: *Mater. Sci. Forum*, 2000, vol. 329, pp. 65-72.
9. L.R. Morris and M. Ryvola: *Microstr. Sci*., 1981, vol. 9, pp. 141-50.
10. J.A. Eady and L.M. Hogan: *J. Cryst. Growth*, 1974, vol. 23, pp. 129-35.
11. A. Kamio: *Proc. Japan–US Cooperative Science Program Seminar on Solidification Processing of Advanced Materials*, Oiso, Japan Society for the Promotion of Science and NSF, Kanagawa, Japan, 1989, p. 195.
12. S.E. Battersby, R.F. Cochrane, and A.M. Mullis: *J. Mater. Sci*., vol. 35, pp. 2000, 1365-73.
13. S.E. Battersby: Ph.D. Thesis, University of Leeds, Leeds, 1997.
14. K.I. Dragnevski: Ph.D. Thesis, University of Leeds, Leeds, 2002.
15. K. Eckler and D.M. Herlach: *Mater. Sci. Eng. A*, 1994, vol. 128, pp. 159-62.
16. A. Karma: *Int. J. Non-Equilibrium Processing*, 1998, vol. 11, pp. 201-33.
17. A.M. Mullis and R.F. Cochrane: *Int. J. Non-Equilibrium Processing*, 2000, vol. 11, pp. 283-97.
18. A.M. Mullis and R.F. Cochrane: *J. Appl. Phys*., 1997, vol. 82, pp. 3783-90.
19. S.E. Battersby, R.F. Cochrane, and A.M. Mullis: *J. Mater. Sci*., 1999, vol. 34, pp. 2049-56.
20. K. Kuribayashi and T. Aoyama: *J. Cryst. Growth*, 2002, vols. 237–239, pp. 1840-43.
21. H.J. Wood, J.D. Hunt, and P.V. Evans: *Acta Mater*., 1997, vol. 45, pp. 569-74.